JOURNAL OF MATERIALS SCIENCE 26 (1991) 1131–1136

Application of scanning tunnelling microscopy to fatigue and fracture

J. LANKFORD
Southwest Research Institute, 6220 Culebra Road, San Antonio, Texas, USA 78228-0510
M. LONGMIRE
Digital Instruments Inc., 135 Nogal Drive, Santa Barbara, California, USA 93110

The scanning tunnelling microscope (STM) is applied to the characterization of fine-scale details associated with the fatigue fracture surface of a steel alloy, and with fibre-coating microfracture in a fibre-reinforced metal matrix composite. Results are compared with those obtained by conventional scanning electron microscopy, and discussed in terms of implications for exploiting the STM in the study of deformation and fracture.

1. Introduction

Since its invention in 1981 [1], the scanning tunnelling microscope (STM) has undergone rapid development, and has been applied to a variety of problems for which it appears to be uniquely suited. A few of these include [2–4] the elucidation of the atomic arrangements of surfaces, characterization of the dynamics of chemical processes (corrosion, electroplating), and the study of large organic molecules such as DNA. Most of these applications have capitalized on the sub-atomic scale spatial resolution of the STM, which permits the accurate mapping of discrete atoms on, or composing, surfaces. However, the instrument also is capable of providing information over a coarser range which, nevertheless, is beyond the capability of the scanning electron microscope (SEM). This ability already has been exploited in the texturing of magnetic media, and in profiling grooves and pits in compact discs, optical discs, and integrated circuits. It has only recently become clear that this size range corresponds to an important microfracture regime which is difficult to explore via scanning electron microscopy (SEM).

Ranges of the two techniques in terms of both lateral and vertical resolution are shown in Fig. 1 (derived from Kuk and Silverman [5]). Basically, the scanning electron microscope is limited to approximately 10 nm in both its vertical and horizontal resolution. This means, of course, that even rather large planar features may not be visible as such if their boundaries contain no discrete vertical elements on a scale of at least 10 nm. Unfortunately, there are many practical situations, especially ones involving fatigue and fracture, for which the vertical elevations required for SEM discrimination can fall into this "fuzzy" realm. Conversely, it is evident (Fig. 1) that the STM easily overlaps the lower range of the SEM, and offers a complementary means of exceeding the limitations of the latter.

The objective of this paper is to demonstrate the ability of the scanning tunnelling microscope to shed new light in an area of research currently dominated by the scanning electron microscope. Examples involving both fatigue and fracture are presented. However, it will be shown that the future of the STM, insofar as regards this type of research, is intimately related to its eventual incorporation into the scanning electron microscope itself.

2. Background information

2.1. Problem areas

The present application of STM is focused on two problems of current interest, one related to the growth of fatigue cracks in metal alloys, the other involving the role of interfaces in the fracture of composite materials. Both revolve around parameters whose vertical and horizontal scale poses a severe challenge to the SEM.

A question of great fundamental significance regards the nature of the events which occur during fatigue crack extension in the near-threshold cyclic stress intensity (ΔK) regime. Considerable evidence exists [6–8] which supports the idea that this process is discontinuous, i.e. many cycles corresponding to local damage accumulation are required before the crack tip lengthens on a single load cycle. For certain materials, the latter event creates a fracture surface marking, i.e. a striation. It has been noted [7] that in a number of cases, there exists near the threshold a ΔK-independent minimum striation spacing, whose dimension is comparable to the crack tip dislocation subcell size. Under such low $-\Delta K$ conditions, the resolution of striations via SEM is difficult; they are very fine in size, and, in addition, often are abraded by Mode II sliding [6] during crack tip opening and closure.

Currently, it is known that aluminium [6, 7], magnesium [7], and ferritic steel [8] alloys display the near-threshold ΔK-independent striation spacing/dislocation subcell size correlation outlined above. However, while it also is known that the austenitic stainless steels form crack tip subcells [9, 10], to date their

0022–2461/91 $03.00 + .12

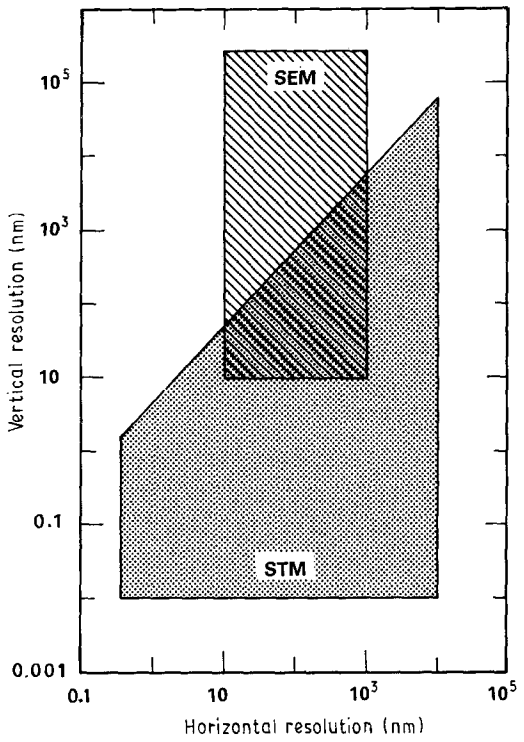

Figure 1 Relative resolution capabilities of SEM compared to STM.

near-threshold fatigue fractography has not been successfully characterized via SEM. One of the present objectives is to accomplish this using STM.

The other problem to be considered involves the role of carbon coatings in controlling the fracture of SiC fibres and, hence, the fracture of SiC fibre-reinforced composites. It has been established [11] that fibres coated with carbon are roughly twice as strong as uncoated ones, and the suggestion has been offered [12] that this result is due to the masking of stress-concentrating micronotches on the fibre surfaces. This saw-tooth profile was inferred from transmission electron microscopy (TEM) thin foil cross-sections of coated fibres [12]. The second objective is thus to characterize fracture surfaces in which cracks have run along the fibre-coating interface. Particular attention will be paid to the fibre topography, and an effort will be made to quantify its stress-raising propensity.

3. Scanning tunnelling microscopy

It is not the purpose here to present a detailed description of the scanning tunnelling microscope; this would constitute a paper in itself, and the interested reader may consult any of a number of excellent reviews. Two of particular relevance to the work at hand are the recent articles by Hansma *et al.* [2], and by Kuk and Silverman [5]. However, it is pertinent to consider a few of the factors involved in using the STM.

The principals of operation of an STM are simple. Basically, an extremely (usually atomically) sharp conducting tip is scanned about over the surface of a conducting specimen via an X, Y, Z piezoelectric translator. Separation between the tip and the surface of the sample is feedback-controlled by the voltage applied to the Z-piezo. The feedback circuit measures and maintains the small electrical current due to electrons tunnelling across the gap under the influence of a low (millivolt–volt) bias voltage at the tip. As the tip is scanned laterally across the surface, its distance above the surface is controlled so as to maintain a constant tunnelling current; a topograph of the surface in X and Z derives from the Z-piezo voltage recorded during the scanning trajectory of the tip. Repeating this scan for various Y-settings yields a three-dimensional view (known as a tunnelling image) of the surface composed of multiple X–Z line scans. It is possible to operate on these data to produce computer-rendered grey-tone images which resemble those obtained by conventional scanning electron microscopy.

Difficulties in STM work generally arise from the fact that the tunnelling current flows only when the tip is within 1 to 2 nm of the surface. This is caused by the exponential decrease in current as the tip moves away from the surface; thus, for fine-scale atomic-resolution work, vibration isolation and thermal drift are major considerations [3]. In the present case, the rigidity of the microscope framework and, especially, the speed of its feedback system, are paramount concerns. The tip must scan rapidly enough to produce an image within a reasonable amount of time, commensurate with its ability to dodge, as it flies over the sample, the suddenly appearing large-scale (relative to the tip-to-sample separation) obstacles characteristic of a fracture surface. This problem obviously is compounded by the inability of the operator to position accurately the tip of a stand-alone STM.

4. Experimental procedure

A single-edge-notched specimen of 316 stainless steel was pre-cracked at a cyclic stress intensity (ΔK) of 25 MPa $m^{1/2}$. Subsequently, standard load-shedding procedures were followed in order to approach the apparent fatigue threshold; at this point, the minimum driving force for which crack extension could be discerned was $\Delta K = 6.5$ MPa $m^{1/2}$. The specimen was then broken open for fractographic analysis.

Similarly, a beam-type Ti_3Al intermetallic alloy specimen reinforced with SCS-6 (AVCO, Specialty Materials Division, Lowell, Massachusetts) SiC fibres was notched prior to dynamic fracture. The fibres were oriented with their axes parallel to the direction of subsequent crack growth from the base of the notch, which was accomplished by subjecting the specimen to a Charpy impact loading.

The fracture surfaces of both specimens were characterized by SEM and STM (Nanoscope II, Digital Instruments Inc., Goleta, California). In the latter case, data were obtained in air using the constant current mode. Images were recorded by photographing either a storage oscilloscope screen displaying the computer-generated STM analogue of an SEM secondary image, or a computer monitor displaying multiple X(in-plane location)–Z(vertical displacement) profiles. Electrochemically etched tungsten tips were used in the study; tip positioning relative to the

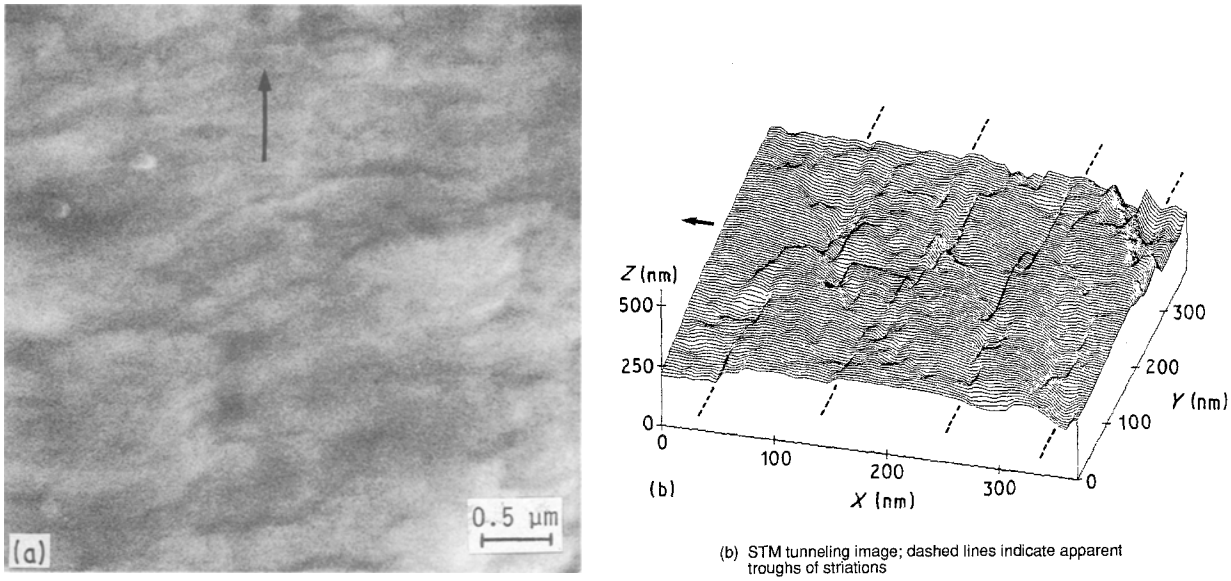

(b) STM tunneling image; dashed lines indicate apparent troughs of striations

Figure 2 Fatigue striations in 316 stainless steel at $\Delta K = 6.5$ MPa $m^{1/2}$; arrows indicate direction of crack growth. (a) SEM image, (b) STM tunnelling image; dashed lines indicate apparent troughs of striations.

fracture surface was performed using a × 25 optical microscope. The latter factor, combined with the fact that the scan range over the in-plane X and Y co-ordinates was only 2 μm × 2 μm, meant that it was difficult to pin-point the location of the tip relative to fine-scale features identified previously via SEM or high-magnification optical microscopy, and equally difficult to locate them, if missed, by scanning about over the extremely limited STM range.

It should be noted that the surfaces studied here were extremely rough in comparison with conventional STM operation, and moreover, were relatively random in their roughness. Thus, the sample was difficult to scan, because the surface feature heights and the limited vertical range of the head permitted only small-area scanning. Moreover, it was difficult to place the tip laterally using low-magnification optical microscopy, so that tip damage due to contact with local, lateral micro-outcroppings was a persistent problem.

5. Results

5.1. Fatigue crack growth

Scanning electron microscopy of near-threshold stainless steel fatigue fracture surfaces produced rather fuzzy images of more-or-less periodic markings (Fig. 2a). It certainly would be difficult to obtain reliable striation spacings from such a photomicrograph, and virtually impossible to assess the actual profiles of the striations. This picture, corresponding to an original magnification of × 20 000 in the SEM, contrasts sharply with the STM line scan image shown in Fig. 2b.

The latter, which is near (controlled by the × 25 positioning cathetometer) the region shown in Fig. 2a, was obtained at an original magnification of × 200 000. It can be seen that lying normal to the direction of crack propagation are roughly parallel depressions spaced on the order of 100 nm, i.e. 0.1 μm; the average depth of these troughs is approximately 20 nm. Unlike "classic" fatigue striations, the markings appear to be discontinuous in certain places, as though they had been smeared over.

The average spacing between periodic markings for several such sets are shown (Fig. 3) plotted against ΔK, together with striation spacings via SEM [13], and the macroscopic (average) crack growth rate [13]. Extrapolating the macroscopic crack growth rate to $\Delta K = 6.5$ MPa $m^{1/2}$ yields a predicted rate of extension of 7×10^{-12} m/cycle, more than four orders of magnitude smaller than the crack-tip jump distance inferred from the STM data. Moreover, the STM results deviate from the easier-to-resolve striation spacings obtained using the SEM at higher ΔK levels, and suggest a transition, at $\Delta K \simeq 13$ MPa $m^{1/2}$, to ΔK-independent striation markings on the order of 0.1 μm wide. The possible physical basis for this limiting size scale will be considered in the discussion.

5.2. Fibre/coating interface fracture

A typical SEM image of the intermetallic composite fracture surface is shown in Fig. 4a. It is evident that several types of fracture are involved, including matrix/coating (M/C) separation, interlaminar coating (IC) failure, and cracking near the fibre/matrix (F/M) boundary. It is the last case which is of most interest in the present instance.

Close inspection of the two regions of the fibre separated by the "line" AB in Fig. 4b reveals that they are physically different. In particular, what appear to be more-or-less circumferential serrations on the body of the fibre apparently end at the line; only the overall "bumpy" surface is preserved above AB, albeit somewhat fuzzily. This suggests that AB represents the edge of part of the coating which remains adherent to the fibre, thereby filling in the serrations.

Scanning tunnelling microscopy shows that this is indeed the case and, moreover, quantifies the situ-

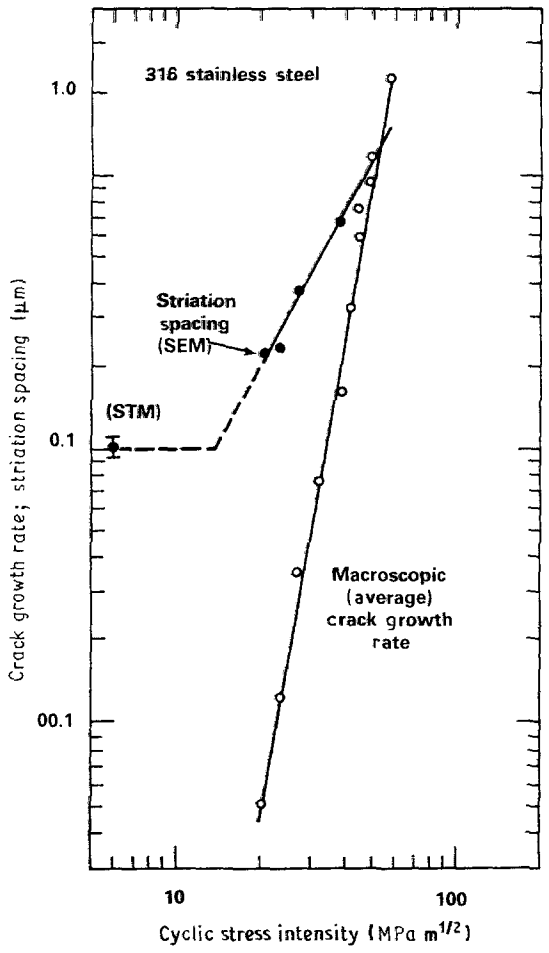

Figure 3 Fatigue crack growth rate and striation spacings in 316 stainless steel.

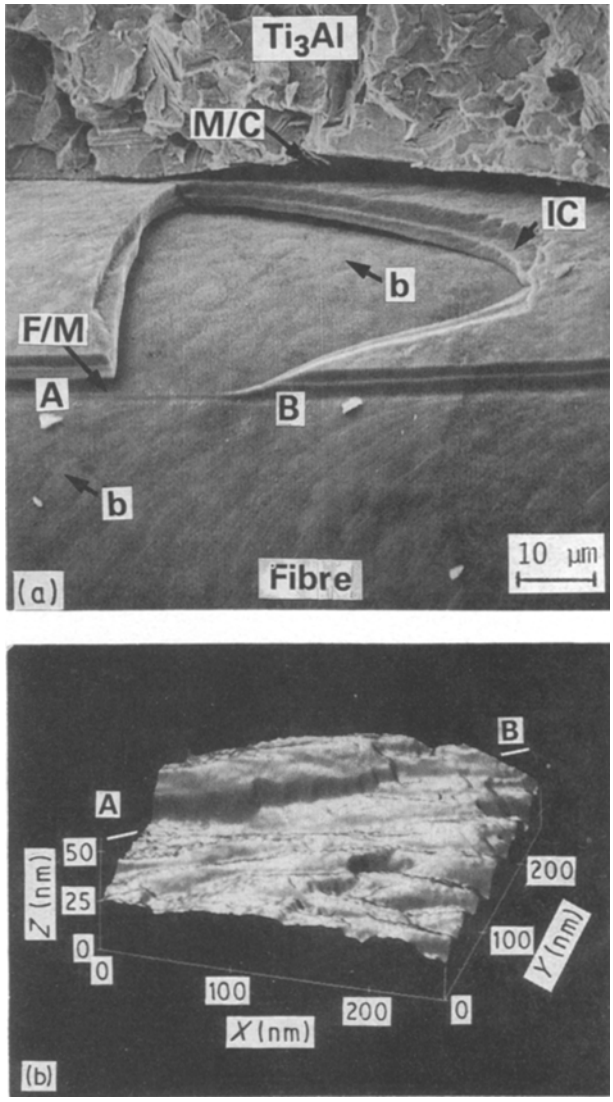

Figure 4 Fracture surface of Ti_3Al/carbon-coated SiC fibre-reinforced composite. (a) SEM image of various fracture modes associated with metal matrix, fibre and coating. Bumps "b", on the base fibre are replicated by the thin layer of coating remaining within the approximately oval tear, while the circumferential fibre serrations are not. Region of major interest: apparent boundary along AB. (b) Computer-rendered STM image of local region along AB; fibre axis is along the Y direction. The plateau above AB consists of coating layer I, while the YZ plane at $X = 250$ nm shows a cross-section of several fibre serrations.

ation. By tediously moving the STM tip about, it finally was possible to locate (Fig. 4b) a site crossed by AB. The latter corresponds to a plateau, approximately 15 nm high, lying on top of a serrated landscape. The profile of the serrations, roughly normal to the Y-(fibre) axis, is manifest in the Y–Z section at $X = 250$ nm in Fig. 4b. Measurement along such profiles indicates an average period of 50 nm, an average depth of 9 nm, and a radius at the base of a typical serration equal to 6.5 nm.

6. Discussion

6.1. Fatigue crack growth

The near-threshold fatigue markings discernible by means of STM are consistent with current ideas regarding fatigue crack growth. Their discontinuous nature, for example, is suggestive of rubbing due to mixed mode crack tip opening/closing [6]. Davidson has shown explicitly [14], by means of stereo-imaging strain analysis, that near the threshold in most, if not all, engineering alloys, crack tip opening shifts toward Mode II.

The apparent striation spacing obtained by STM, ~0.1 μm, is in excellent agreement with the TEM crack tip subcell measurements by Bathias [9, 10] for 316 stainless steel under equivalent conditions. This suggests, of course, that striations formed under near-threshold conditions do so via subcell breakdown. Moreover, based on the orders of magnitude difference between the macroscopic crack growth rate and the average striation spacing, the breakdown/crack extension process must be highly discontinuous, whereby each such event, resulting in one striation, requires thousands of fatigue cycles. This is the same sort of behaviour which has been documented recently by Roven *et al.* [8] for ferritic steels, the major difference being that in the latter case, the striations formed under near-threshold conditions possess sufficient topographical relief to permit their resolution via SEM.

6.2. Fibre/coating interface fracture

The structure of silicon carbide filaments has been well-characterized by Nutt and Wawner [12] and Wawner [15]. For present purposes, it suffices to

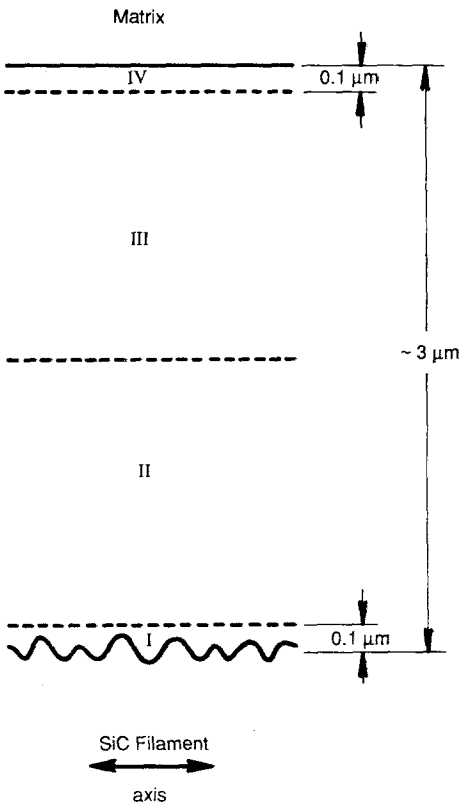

Figure 5 Schematic sectional view of the coating structure, showing various layers (not to scale).

observe that the carbon–silicon protective coating on the SiC fibre consists of several distinct layers, as shown schematically in Fig. 5. Layers II and III comprise the bulk of the coating, and are readily visible in Fig. 4a (the locale of the IC failure); they both consist primarily of turbostratic pyrolitic carbon, the boundary between them reflecting a characteristic sudden increase in the concentration of hydrocarbon gas during deposition. Layers I and IV are thin (~ 0.1 μm), and consist basically of small crystallites of SiC embedded in an isotropic carbon matrix.

From Fig. 4b, it appears that the fracture associated with the first layer has occurred only about 15 nm above the SiC substrate. This is interesting, in that layer I is usually thicker than this [12, 15]. However, the fact that the "bumps" on the fibre are replicated on the coating in Fig. 4a suggests that the coating fracture plane is indeed a structural transition zone, rather than an intra-layer I failure.

However, the principal question to be addressed here concerns the stress reduction of the serrations presumably affected by the presence of the coating. From elementary fracture mechanics, the stress raising capability of a notch of depth, d, and radius, r, can be written

$$\sigma_{max} = 2\sigma_A\left(\frac{d}{r}\right)^{1/2} \quad (1)$$

where σ_A is the applied stress normal to the notch and σ_{max} is the enhanced local stress at the notch tip. Judging from the STM measurements that the serrations* circumscribing the fibres constitute surface micronotches of depth 9 nm and radius 6.5 nm, σ_{max} turns out to be $2.17\,\sigma_A$. This result clearly is compatible with the measured [11] (approximate) twofold strengthening of individual fibres upon coating them with carbon-silicon, i.e. the coating fills up the notches and effectively removes them.

6.3. Implications

It is hoped that this brief study serves to demonstrate the potential of scanning tunnelling microscopy to add a new dimension to the study of fatigue and fracture. Although the technique poses formidable difficulties, the information which it may provide seemingly is worth the effort required to obtain it.

Probably the greatest drawback to the use of the STM by fracture-oriented researchers is the fact that positioning of the tip is basically blind. What is needed is the literal incorporation of the STM into the SEM, so that the latter can be used first to establish local regions of particular interest or importance, and then to guide the STM tip down to a safe position just above such local landmarks. Preliminary efforts toward this goal have been implemented [16, 17], but results have been inconclusive, and at this time, no commercial SEM/STM is available.†

Clearly, however, considerations of paramount importance must include effective vibration isolation, and a design which permits the observation of the STM tip by the SEM detector. It already has been demonstrated [17] that it is possible to operate the STM and the SEM simultaneously, provided that the set current for the STM is at least twice as large as the SEM beam current.

Most STM work to date has fallen within the purview of surface physics, whose practitioners are interested in individual atoms. Thus, most such studies have been performed within very high vacuum (usually on the order of 10^{-10} torr or 133.3×10^{-10} Pa) systems, such as ion pumps. While this is not a necessity in the present instance, a clean, non-oil diffusion pump environment would be required. Otherwise, breakdown of back-streaming oil molecules will produce surface contaminants liable to compromise results.

It should be noted that scanning tunnelling microscopy can be performed in many environments, aside from high vacuum or the ambient atmosphere characteristic of the present experiments. Good STM images have been obtained in a variety of electrolytes and liquids, including water [18]. In this case, the tip is totally immersed in the liquid, and tunnelling occurs within the latter medium.

* The serrations represent the intersections of the outermost SiC subgrains of the filament [12].

† The interested reader should note the very recent and important paper by H. Fuchs and R. Laschinski (*Scanning* **12** (1990) 126), in which they describe the combination of a miniature "pocket" STM with a standard SEM. Their implementation of the piezo-tripod STM configuration, versus the alternative cylindrical tube-scanner, is the optimum design to permit SEM visualization of the tip. The obvious success of this combination reinforces the present conclusions regarding the power and potential of STM/SEM symbiosis.

Finally, Bonnell and Clarke [4] have demonstrated that under certain circumstances, the STM is applicable to poor conductors such as ceramics. In the long run, characterization of the latter probably will devolve to the closely allied technique of atomic force microscopy [2]. This even more recent development is likewise amenable to SEM incorporation.

Acknowledgements

The authors are grateful for the support of the Air Force Office of Scientific Research, under Contract no. F49620-89-C-0032, and also for support provided by Southwest Research Institute. The assistance of John Campbell and James Spencer in performing the fatigue and fracture tests is greatly appreciated.

References

1. G. BINNING and H. ROHRER, *Helv. Phys. Acta* **55** (1982) 726.
2. P. K. HANSMA, V. B. ELINGS, O. MARTI and C. E. BRACKER, *Science* **242** (1988) 209.
3. J. A. GOLOVCHENKO, *ibid.* **232** (1986) 48.
4. D. A. BONNELL and D. R. CLARKE, *J. Amer. Ceram. Soc.* **71** (1988) 629.
5. Y. KUK and P. J. SILVERMAN, *Rev. Sci. Instrum.* **60** (1989) 165.
6. J. LANKFORD and D. L. DAVIDSON, *Acta Metall.* **31** (1983) 1273.
7. N. M. GRINBERG, *Inst. J. Fat.* **6** (1984) 229.
8. H. J. ROVEN, M. A. LANGOY and E. NES, in "Fatigue 87", edited by R. O. Ritchie and E. A. Starke Jr (Engineering Materials Advisory Services, Cradley Heath, UK, 1987) p. 175.
9. C. BATHIAS, *Mem. Sci. Rev. Metall.* **67** (1971) 233.
10. *Idem., ibid.* **67** (1971) 233.
11. R. L. CRANE and V. J. KRUKONIS, *Ceram. Bull.* **54** (1975) 184.
12. S. R. NUTT and F. E. WAWNER, *J. Mater. Sci.* **20** (1985) 1953.
13. C. BATHIAS and R. M. PELLOUX, *Met. Trans.* **4** (1973) 1265.
14. D. L. DAVIDSON, *Mater. Sci. Engng* **60** (1983) 225.
15. F. E. WAWNER, in "Fibre Reinforcements for Composite Materials", edited by A. R. Bunsell (Elsevier, Amsterdam, 1988) p. 371.
16. T. ICHINOKAWA, Y. MIZAZAKI and Y. KOGA, *Ultamicroscopy* **60** (1989) 165.
17. CH. GERBER, G. BINNING, H. FUCHS, O. MARTI and H. ROHRER, *Rev. Sci. Instrum.* **57** (1986) 221.
18. S. M. LINDSAY, T. THUNDAT, L. NAGAHARA, U. KNIPPING and R. L. RILL, *Science* **244** (1989) 1063.

Received 20 October
and accepted 1 December 1989